Princeton Plasma Physics Laboratory

PPPL- 4371

PPPL- 4371

Scaling of radial propagating structures in the scrape-off layer of the National Spherical Torus Experiment (NSTX)

T. Windisch, O. Grulke, S.J. Zweben and R. J. Maqueda

December, 2008

Prepared for the U.S. Department of Energy under Contract DE-AC02-76CH03073.

Princeton Plasma Physics Laboratory
Report Disclaimers

Full Legal Disclaimer

Trademark Disclaimer

PPPL Report Availability

Princeton Plasma Physics Laboratory:

http://www.pppl.gov/techreports.cfm

Office of Scientific and Technical Information (OSTI):

http://www.osti.gov/bridge

Related Links:

U.S. Department of Energy

Office of Scientific and Technical Information

Fusion Links

Scaling of radial propagating structures in the scrape-off layer of the National Spherical Torus Experiment (NSTX)

T. Windisch, O. Grulke

Max-Planck-Institute for Plasma Physics, EURATOM Association, D-17491 Greifswald, Germany

E-mail: thomas.windisch@ipp.mpg.de

S.J. Zweben

Princeton Plasma Physics Laboratory, Princeton, New Jersey, 08540

R. J. Maqueda

Nova Photonics, Princeton, New Jersey, 08540

Abstract. The radial propagation of spatiotemporal turbulent structures in the scrape-off layer of the National Spherical Torus Experiment [M. Ono, M.G. Bell, R.E. Bell, *et al.* Plasma Phys. Control. Fusion **45**, A335 (2003)] is investigated. Two-dimensional spatiotemporal imaging of the D_α emission intensity is used to observe the fluctuation structures in the poloidal plane perpendicular to the ambient magnetic field. Turbulent structures are extracted and the individual properties such as velocity, spatial scale and amplitude are determined. The typical poloidal scale of the structures is $k_\theta = 0.5\,\mathrm{cm}^{-1}$. The poloidal and radial structure velocities are $< 5\,\mathrm{km/s}$ and $\approx 1\,\mathrm{km/s}$, respectively. The radial velocities do not vary significantly with their spatial size within this set of data.

PACS numbers: 52.35.Kt,52.35.Ra,52.25.Xz

1. Introduction

The plasma flow into the scrape-off layer (SOL) of tokamaks is strongly governed by turbulent transport across the confining magnetic field, the so-called anomalous transport [1, 2, 3, 4]. This turbulent cross-field transport leads to a broadening of the time-averaged density profile, it has a strong impact on the divertor efficiency and might affect key reactor issues like helium "ash" removal. A special feature of this convective particle flux in the SOL are intermittent density bursts, characterized by a non-Gaussian probability distribution function (PDF), which are ascribed to spatiotemporal large-amplitude turbulent structures, the so-called blobs. They propagate radially outwards across the SOL with a velocity of typically 1-10% of the ion sound speed and eventually reach the first wall [5, 6, 7, 8, 9].
Blobs are localized in the poloidal plane but they are elongated along the magnetic field lines, thereby forming filaments with $k_\parallel/k_\perp \ll 1$ [8]. It was shown that blobs contribute significantly to the radial transport in the SOL [10]. Common models addressing the radial propagation of blobs in the SOL of fusion devices rely on the curvature of the magnetic field [9, 11]. The curvature and $\nabla\vec{B}$-drifts give rise to a charge polarization of the blob, which results in a radial $\vec{E}\times\vec{B}$-drift of the blobs directed radially outwards. Crucial for the charge build-up process is the blob's parallel dynamics. In the SOL a parallel flow along the magnetic field lines towards material surfaces can counterbalance the charge polarization and thus inhibits radial blob propagation [12]. A damping of the potential perturbation associated with the blob may also occur in regions with a specific magnetic field topology such as X-points, where cross-field currents are greatly increased [13]. For each of these damping regimes of the blob's radial propagation the models predict a scaling of the radial blob velocity [14], which depends on the blob specific parameters as spatial scale size and relative fluctuation amplitude.
In this paper two-dimensional measurements of the plasma density fluctuations in the plasma edge and SOL region in the NSTX tokamak using gas-puff imaging (GPI) diagnostic are presented. Turbulent structures are extracted and their radial velocities are determined as a function of their relative fluctuation amplitude and spatial scale. The findings are compared with the individual model predictions. The paper is organized as follows: SEC. 2 outlines the discharge configuration, the diagnostic equipment, and the data processing to extract the turbulent structures. In SEC. 3 the basic characteristics of the spatiotemporal fluctuations are discussed. The results for individual structures propagating from the edge into the limiter shadow are presented in Sec. 4, together with a statistical analysis of the scaling of the radial blob velocity. The results are summarized and discussed in Sec. 5.

2. Experimental setup

The measurement results presented in this paper are obtained from NBI-heated L-mode discharges with moderate heating power P_{NBI} =2-4 MW, a toroidal magnetic

Table 1. NSTX plasma parameters in the plasma edge and SOL as derived from Thomson scattering measured along the outer midplane.

Parameter	Separatrix ($r = r_{sep}$)	SOL ($r = r_{sep} + 8\,\mathrm{cm}$)
electron density n_e [$10^{19}\,\mathrm{m}^{-3}$]	0.7	0.05
electron temperature T_e [eV]	20	3
drift scale ρ_s [mm]	1.5	0.58
ion sound speed c_s [km/s]	44	17

field $B = 0.3\,\mathrm{T}$ with near double-null configuration and a plasma current of 800 kA. For detailed information about the discharge configuration the reader is referred to Ref. [15]. Typical plasma parameters in the plasma edge and SOL for the considered shots (113733-113744) are compiled in Tab. 1.

Spatiotemporal fluctuations in the plasma edge and SOL region are measured using gas puff imaging technique (GPI) [7, 6]. A fast framing Princeton Scientific Instruments PSI5 camera (frame rate 250 kHz, 300 frames memory, 64× 64 pixel) measures the visible D_α line emission (656 nm) from a localized deuterium gas puff at the outer midplane. The field-of-view spans over 23 × 23 cm radially and poloidally, centered radially near the magnetic separatrix. The view is tangentially to the local magnetic field in order to resolve the radial and poloidal structure of the fluctuations perpendicular to the ambient magnetic field. Detailed information about the GPI system used for the presented NSTX shots can be found in Ref. [15]. The orientation of the GPI field-of-view with respect to the separatrix and limiter edge is shown in Fig. 1. It covers a radial and poloidal range including the edge region and the entire SOL. The light emission intensity S_α of the D_α line (656 nm) is proportional to the neutral gas density n_0 and depends nonlinearly on the electron temperature T_e and the electron density n_e [7], $S_\alpha \sim n_0 n_e^{\alpha_1} T_e^{\alpha_2}$. A detailed comparison of experimentally data with Degas 2 neutral transport code calculations can be found in [16, 17]. For the considered shots discussed in this paper the exponents α_1 and α_2 vary between $0.8 - 3$ across the GPI field-of-view [18]. The fluctuations of the D_α emission intensity $\tilde{D}_\alpha$ can be attributed to either fluctuations in n_e, T_e, n_g, or all of them. If the variations of the neutral gas density are assumed to occur on a much larger time scale than the turbulent fluctuations $\tilde{D}_\alpha$ depends on the electron density and temperature fluctuations only [8]. The analysis of the latter contributions is simplified since electron density and temperature fluctuations are in phase as shown experimentally [19, 20] and in numerical simulations [21].

The signal processing to extract spatiotemporal structures from the raw camera images is divided into pre-processing and tracking of the extracted structures. The pre-processing of the raw camera images includes bandpass filtering with passband $f_1 < f < f_2$, where $f_1 = 1\,\mathrm{kHz}$ and $f_2 = 115\,\mathrm{kHz}$, respectively, to remove the dc-component and limit the fluctuation frequency below the Nyquist limit. To reduce the random pixel noise due to the neutron/gamma background for each frame a 2D-median filtering over 3 pixel and a 2D-singular value decomposition are applied, where the 3

largest singular values are taken. After pre-processing, the camera images are filtered with respect to an amplitude and area threshold to extract the turbulent structures. The condition for the amplitude was set to $1\,\sigma$, where σ is the standard deviation of each pixel time series and the condition for the area was set to 20 pixel, which corresponds to $2.9\,\mathrm{cm}^2$. All identified objects of each frame are labeled and the individual properties (area, amplitude, center of mass position, position of maximum amplitude, bounding box, orientation) are determined. The area of a structure is defined as the area where the amplitude of the structure exceeds 60 % of the peak structure amplitude. To trace the structures for consecutive frames we utilize the bounding box of the detected structures and their center of mass. The bounding box is the minimum rectangular which encloses the structure. If the center of a structure in frame $i+1$ is found within the bounding box of a structure in frame i we treat them as related. This criterion implies an upper velocity limit for which a propagating structure can be clearly identified in two consecutive frames using the described method, which is $\sim 4-5\,\mathrm{km/s}$ for small scale structures ($5\,\mathrm{cm}^2$) and $\sim 5-6\,\mathrm{km/s}$ for larger scale structures ($10\,\mathrm{cm}^2$). Typical poloidal and radial structure velocities for the NSTX SOL region are $\leq 5\,\mathrm{km/s}$ and $1\,\mathrm{km/s}$, respectively [15]. The estimated velocities strongly depends on the condition that determines the area of the structure affecting the center position for non-symmetric structures. Instead of considering the position of the maximum amplitude of the structure as a measure of its center position the center of mass of the entire structure is recognized to account for dynamical changes of the structure's shape during propagation.

3. Characterization of fluctuations

An example of pre-processed PSI5 camera images is shown in Fig. 2 for six time instants spanning over $\Delta t = 100\,\mu\mathrm{s}$. For all time instants a propagating coherent structure is clearly observed. The structure propagates from the plasma edge poloidally downwards in the direction of the ion diamagnetic- and $\nabla\vec{B}$-drift and radially outwards into the limiter shadow across the SOL. In the plasma edge and SOL the structure is poloidally distorted with a poloidal and radial extensions of 8 cm and 6 cm, respectively. As the structure approaches the limiter shadow ($r > 153\,\mathrm{cm}$) it decreases in size and develops towards a circular shape with a radius $r = 2.2\,\mathrm{cm}$.

The characteristic poloidal size of the structures in the GPI field-of-view is investigated in detail by applying a wavelet spectral analysis. For each of the 64 radial pixel positions the poloidal wavenumber spectrum is estimated using the continuous Morlet wavelet transform. The resulting radially resolved poloidal wavenumber spectrum averaged over the PSI5 acquisition time (1.2 ms) is shown in Fig. 3a. In the plasma edge and SOL region the fluctuation energy is centered at a poloidal wavenumber $k_\theta \approx 0.5\,\mathrm{cm}^{-1}$, which corresponds to a typical poloidal structure size of $\approx 6\,\mathrm{cm}$. This is in agreement with the observations of the individual structure (Fig. 2). Structures with smaller poloidal scale sizes ($k_\theta > 1.5\,\mathrm{cm}^{-1}$) occur predominantly close to the separatrix while in the edge plasma and limiter shadow mainly structures with larger poloidal

scales contribute to the fluctuation energy. A temporally resolved poloidal wavenumber spectrum obtained in the SOL is shown in Fig. 3. The radial position, at which the spectrum is estimated, is indicated in Fig. 3a at $r = 153\,\mathrm{cm}$. Here, the propagating structures are observed as sporadic events with peaks at $k_\theta \approx 0.5\,\mathrm{cm}^{-1}$ but extend to $k_\theta \approx 2 - 3\,\mathrm{cm}^{-1}$. Note that the statistical properties of the wavenumber spectrum are analyzed in more detail in Ref. [22] for the same set of NSTX L-mode discharges.

The characteristic poloidal and radial velocities of fluctuations are estimated using the cross-correlation technique (CCF) [23]. Note that in this analysis method the pre-processed camera images are used, i.e., the structures are not extracted and the entire fluctuation spectrum is considered. The D_α-timeseries of one camera pixel is used as a reference and the correlation with all 64×64 pixel is estimated. In order to gain spatially resolved information multiple reference pixel positions are used on an equidistant grid with 12 poloidal and 21 radial reference points. The so-obtained radial evolution of the radial and poloidal correlation lengths, Δ_{rad} and Δ_{pol} are shown in Fig. 4a for time lag $\tau = 0$. The poloidal correlation length decreases from $\Delta_{pol} \approx 7.5\,\mathrm{cm}$ inside the separatrix to $\Delta_{pol} \approx 5\,\mathrm{cm}$ in the separatrix region. In the SOL Δ_{pol} approaches an almost constant value ($\Delta_{pol} \approx 6 - 7\,\mathrm{cm}$) and in the limiter shadow Δ_{pol} decreases to $\approx 5\,\mathrm{cm}$. A similar behavior is observed for the radial evolution of the radial correlation length Δ_{rad}, which decreases from $\approx 10\,\mathrm{cm}$ inside the separatrix to $4 - 5\,\mathrm{cm}$ in the separatrix and SOL region. For each of the 252 reference positions the spatial displacement of the maximum cross-correlation between time lag $\tau_0 = 0$ and $\tau_1 > t_0$ then yields the radial and poloidal velocities of fluctuations. To ensure a significant correlation $\tau_1 = 20\,\mu\mathrm{s}$ is chosen, which is smaller than the autocorrelation time. The result is shown in Fig. 4b. Note that a negative poloidal velocity corresponds to a downward propagation and a positive radial velocity to a propagation directed radially outwards in the representation of Fig. 2. The poloidal velocity peaks at $v_{pol} \approx -4\,\mathrm{km/s}$ in the region of the separatrix ($r_{sep} \approx 146\,\mathrm{cm}$). For larger radii an almost constant poloidal velocity is observed ($v_{pol} \approx -1\,\mathrm{km/s}$). No change of poloidal propagation direction across the separatrix is observed. The radial velocity v_{rad} is close to zero in the separatrix region and $v_{rad} \approx 1\,\mathrm{km/s}$ in the SOL. In the limiter shadow the radial velocity decreases significantly, which might be due to rapid parallel cooling [14]. It is apparent that the increase of the poloidal velocity in the separatrix region (Fig. 4b) coincides with a decrease of the poloidal correlation length in that region. A similar behavior is observed for the radial correlation length and velocity in the separatrix region.

4. Specific properties of individual structures and velocity scaling

To estimate the velocities of the large-amplitude structures they are extracted from the camera images and tracked spatiotemporally in the PSI5 camera field-of-view. The routine for structure extraction was already outlined in SEC. 2. The radial evolution of specific properties as trajectory, velocity, area and amplitude across the SOL into the limiter edge is shown in Fig. 5 for three long-living events. The structures are tracked

radially from $r - r_{sep} \approx 2\,\mathrm{cm}$ for a radial distance of 8-9 cm. In the following the terms mid-SOL ($r - r_{sep} = 5 - 7\,\mathrm{cm}$) and far-SOL ($r - r_{sep} = 7 - 10\,\mathrm{cm}$) are used to distinguish the regions within the SOL. All structures shown in Fig. 5 propagate downwards in the direction of the ion diamagnetic- and ∇B-drift and radially outwards. The evolution of the radial velocity of the structures with increasing distance to the separatrix is shown in Fig. 5b. Typical values of the structure's radial velocity are $0.5 - 1.5\,\mathrm{km/s}$. The poloidal velocity of the structures shown in Fig. 5c peaks close behind the separatrix ($r - r_{sep} \approx 2 - 3\,\mathrm{cm}$) at a value of $2 - 3\,\mathrm{km/s}$ and decreases towards the limiter shadow to $\approx 1\,\mathrm{km/s}$. The radial evolution of the structure amplitudes normalized to the time-averaged background $\bar{D}_\alpha$ emission is shown in Fig. 5.d. The relative amplitude of the structures increases from ≈ 1.5 in the plasma edge region to 3 in the mid-SOL. For larger radii, the amplitude of the structures either decreases or increases. An increase of the relative structure amplitude in the SOL is mainly governed by the radial evolution of the time-averaged radial D_α emission profile $\bar{D}_\alpha$ (cf. Fig. 1) and not associated with the structure amplitude itself.

The radial evolution of the structure area (Fig. 5e) exhibits almost the same characteristics as the normalized amplitude of the structures. Apparently, during structure evolution the radial structure velocity is not controlled by the specific structure properties size and amplitude. From the individual structure properties shown in Fig. 5 a discussion of the scaling of the radial structure velocity with structure amplitude and structure area is rather difficult since no direct relation is observed.

To gain more insight into the scaling of the radial structure velocity with respect to the structure amplitude and structure area, both of these are evaluated statistically over a large number of events. Therefore 11 shots (113733-113744) with similar plasma conditions taken at a single day are considered. For the statistical analysis all extracted structures with a minimum lifetime of $\tau \geq 60\,\mu\mathrm{s}$ (corresponding to 15 frames) are taken into account. The scaling properties of the structure's radial velocity is investigated in a region that covers the plasma edge, the SOL and the limiter shadow ($r - r_{sep} = 0 - 10\,\mathrm{cm}$). All structures found to exist in those regions were extracted and evaluated with respect to an area and amplitude threshold. Since the area of the structure changes during propagation the structure trajectory has to be divided into two-frame ensembles. If the structure area and amplitude fulfills the applied threshold conditions in two adjacent frames an incremental velocity is calculated. Applying this criteria 690 structure ensembles of 55 structures contribute to the statistics for the structure area and amplitude. The resulting probability distribution function (PDF) of the radial structure velocity is shown in Fig. 6 for various area and amplitude thresholds. The lower and upper values for the area and amplitude thresholds are chosen such that the same number of two-frame ensembles contribute to each PDF.

In general the PDFs of the radial structure velocity are broad with a σ-width comparable to the mean value. This feature indicates a strong stochastic element in the evolution of the radial structure velocity. However, slight trends are observed. In Fig. 6a the majority of structure ensembles is centered at $v_{rad} = 0.5 - 1\,\mathrm{km/s}$ for

all area thresholds. However, the PDFs for larger area thresholds ($> 5.5\,\mathrm{cm}^2$) are asymmetric and skewed towards positive velocities. This leads to a slight increase of the mean radial velocity from 660 m/s for the small structures to 740 km/s for the larger structures. In contrast, the trend of higher amplitude structures having a larger radial velocity occurs more pronounced (Fig. 6b). The mean value increases from 480 m/s for low amplitude structures to 1 km/s for high amplitude structures. To estimate a possible influence of the nonlinearity in the D_α emission intensity $S_\alpha \sim n_0 n_e^{\alpha_1} T_e^{\alpha_2}$ on the observed scaling of the radial structure velocity the analysis has been repeated for different exponents varying between $\alpha_{1,2} = 0.8 - 3$. It is found that the scaling results do not vary significantly for the different exponents.

5. Summary and Discussion

In this paper the propagation of spatiotemporal turbulent structures in the plasma edge and SOL were investigated for L-mode plasmas in the NSTX tokamak. The dynamics of the structures is analyzed in a poloidal-radial cross-section perpendicular to the ambient magnetic field using two-dimensional optical D_α GPI diagnostics. Coherent turbulent structures are found to propagate mainly poloidally in direction of the ion diamagnetic- and $\nabla\vec{B}$-drift and radially from the plasma edge across the SOL into the limiter shadow. The poloidal wavenumber spectrum is centered at $k_\theta \approx 0.5\,\mathrm{cm}^{-1}$ which corresponds to a poloidal structure size of ≈ 6 cm. Applying a cross-correlation technique the typical poloidal and radial velocities of the spatiotemporal fluctuation field are found to be $v_{pol} = 1 - 4$ km/s and $v_{rad} \approx 1 - 1.5$ km/s, respectively, which is in agreement with a previous analysis [15]. The specific properties of individual structures are investigated using an extraction and tracking routine. The velocities of the individual structures mainly confirms the results presented in [7, 15, 9] although the incremental velocity estimated from the structure trajectory may vary due to the different definitions of structure area and center position. The radial structure velocity is in agreement with observations from other toroidal machines [5, 23, 8].
From the properties of individual structures the scaling of the radial structure velocity with structure scale size and amplitude cannot be analyzed since no clear relation is observed.

Insight into the scaling is gained using a statistical analysis of long-living structures taking 11 shots with similar discharge conditions into account. In this manner it is observed that the PDFs of the radial structure velocity for various structure amplitudes and areas are broad, which indicates a large stochastic moment in the distribution. However, a qualitative trend of higher amplitude structures being faster is observed but no significant dependence of the radial structure velocity on the spatial size of the structures is found due to large variations in the data. Due to the low significance of the scaling of the radial structure velocity a detailed quantitative comparison with predictions of theoretical models cannot be performed. The observed scaling of the radial velocity with the structure amplitude is expected for different theoretical instability

regimes [14]. In the ballooning regime, in which the structure is not connected along the magnetic field lines with the sheaths at material surfaces due to high plasma resistivity, structures with larger scales and higher amplitudes are expected to have a higher radial velocity. This is not observed here. Note that the ballooning regime is identical with the prediction of the interchange model presented in Ref. [21, 11], in which the formation process of the structure is also considered. One may conclude that the radial propagation of the structure in the SOL is a self-consistent feature of the structure and is not associated with the actual formation process out of the turbulence. However, it has been observed that the amplitude of the structures strongly decreases in the far-SOL and limiter shadow. This cannot be explained by the profiles of the background D_α emission intensity but might be due to a parallel flow to the material boundaries. This would yield evidence that the parallel dynamics must be retained in the model descriptions. Indeed, in the two-dimensional interchange model, a decrease of the radial structure velocity is observed if the parallel currents are explicitly taken into account as a dissipation mechanism. The three-dimensional models which consider this effect (the X-point and sheath-connected instability regime in Ref. [14]) are expected to be valid for NSTX edge plasma parameters [9]. A different set of GPI data of NSTX L-mode shots has been analyzed in Ref. [9]. The observed bounds on the radial blob velocity were found to be consistent with the theoretical predictions of the X-point and sheath-connected instability regime, in which larger structures are expected to have higher radial velocities. A significant double correlation of v_{rad} with blob scale size and distance Δr from the separatrix was found but no clear scaling of v_{rad} with the blob scale size was observed due to large statistical variations in agreement with the findings presented here. This may be a consequence of the fact that the scaling also depends on other structure parameters that were not measured [14], i.e., structure temperature and parallel dynamics of the structure, but may also be due to the statistical nature of the turbulence.

Recently it has been demonstrated by numerical simulations of the self-consistent structure dynamics in the SOL (based on the interchange instability [24]), that the propagation models are not sufficient to describe the structure propagation across the SOL. In these models the structures are treated as isolated structures. It was found that the interaction of background poloidal flows with the structures due to radial electric fields strongly affect their dynamics. Fluctuations in the density, potential and vorticity fields act as a noise that randomly varies the structure dynamics and thereby broadens the distributions of the radial blob velocity.

Acknowledgments

This work was supported in part by U.S. DOE Contract # DE-AC02-76CH03073. We thank D.P. Stotler for discussions concerning the interpretation of the GPI diagnostic and J.R. Myra for discussions concerning the interpretation of the results.

References

[1] P. C. Liewer. *Nucl. Fusion*, 25(5), 543 (1985).
[2] A. J. Wootton, B. A. Carreras, H. Matsumoto, *et al.*. *Phys. Fluids B*, 2(12), 2879 (1990).
[3] F. Wagner and U. Stroth. *Plasma Phys. Controlled Fusion*, 35(10), 1321 (1993).
[4] C. Hidalgo. *Plasma Phys. Controlled Fusion*, 37(11A), A53 (1995).
[5] J. A. Boedo, D. L. Rudakov, R. A. Moyer, *et al.*. *Phys. Plasmas*, 10(5), 1670 (2003).
[6] J. L. Terry, S. J. Zweben, K. Hallatschek, *et al.*. *Phys. Plasmas*, 10(5), 1739 (2003).
[7] S. J. Zweben, R. J. Maqueda, D. P. Stotler, *et al.*. *Nucl. Fusion*, 44, 134 (2004).
[8] O. Grulke, J. L. Terry, B. LaBombard, *et al.*. *Phys. Plasmas*, 13(1), 012306 (2006).
[9] J. R. Myra, D. A. D'Ippolito, D. P. Stotler, *et al.*. *Phys. Plasmas*, 13(9), 092509 (2006).
[10] J. A. Boedo, D. Rudakov, R. Moyer, *et al.*. *Phys. Plasmas*, 8(11), 4826 (2001).
[11] O. E. Garcia, N. H. Bian, and W. Fundamenski. *Phys. Plasmas*, 13(8), 082309 (2006).
[12] D. A. D'Ippolito and J. R. Myra. *Phys. Plasmas*, 10(10), 4029 (2003).
[13] D. A. Russell, D. A. D'Ippolito, J. R. Myra, *et al.*. *Phys. Rev. Lett.*, 93(26), 265001 (2004).
[14] J. R. Myra and D. A. D'Ippolito. *Phys. Plasmas*, 12(9), 092511 (2005).
[15] S. J. Zweben, R. J. Maqueda, J. L. Terry, *et al.*. *Phys. Plasmas*, 13(5), 056114 (2006).
[16] D. P. Stotler, B. LaBombard, J. L. Terry, *et al.*. *J. Nucl. Mater.*, 313-316, 1066 (2003).
[17] D. P. Stotler, D. A. D'Ippolito, B. LeBlanc, *et al.*. *Contrib. Plasma Phys.*, 44(1-3), 294 (2004).
[18] D. P. Stotler. *private communication* (2006).
[19] M. A. Meier, R. D. Bengtson, G. A. Hallock, *et al.*. *Phys. Rev. Lett.*, 8708(8), 085003 (2001).
[20] D. L. Rudakov, J. A. Boedo, R. A. Moyer, *et al.*. *Plasma Phys. Controlled Fusion*, 44(6), 717 (2002).
[21] O. E. Garcia, V. Naulin, A. H. Nielsen, *et al.*. *Phys. Rev. Lett.*, 92(16), 165003 (2004).
[22] M. Agostini, S. J. Zweben, R. Cavazzana, *et al.*. *accepted for publication in Phys. Plasmas* (2007).
[23] J. Terry, S. Zweben, O. Grulke, *et al.*. *J. Nucl. Mater.*, 337-339, 322 (2005).
[24] P. Ghendrih, Y. Sarazin, G. Attuel, *et al.*. *J. Nucl. Mater.*, 337-339(1-3), 347 (2005).

List of Figures

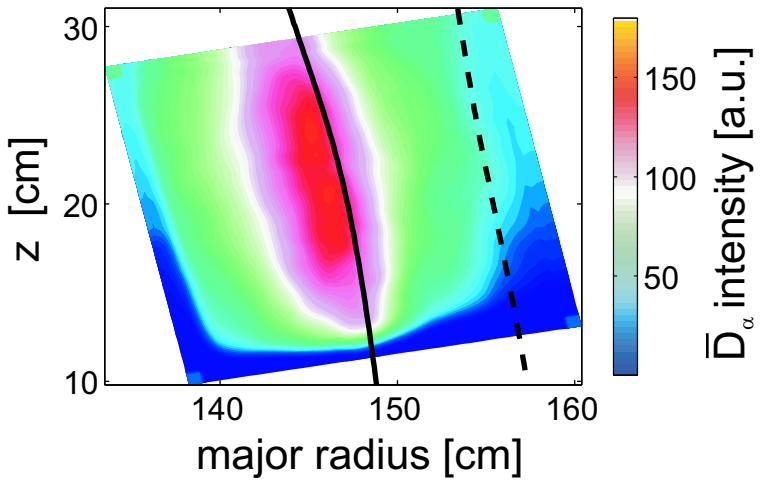

Figure 1. Time-averaged D_α emission $\bar{D}_\alpha$ for shot 113734. The solid black line corresponds to the position of the magnetic separatrix derived from the free-boundary equilibrium reconstruction code LRDFIT. The dashed line corresponds to the position of the limiter edge.

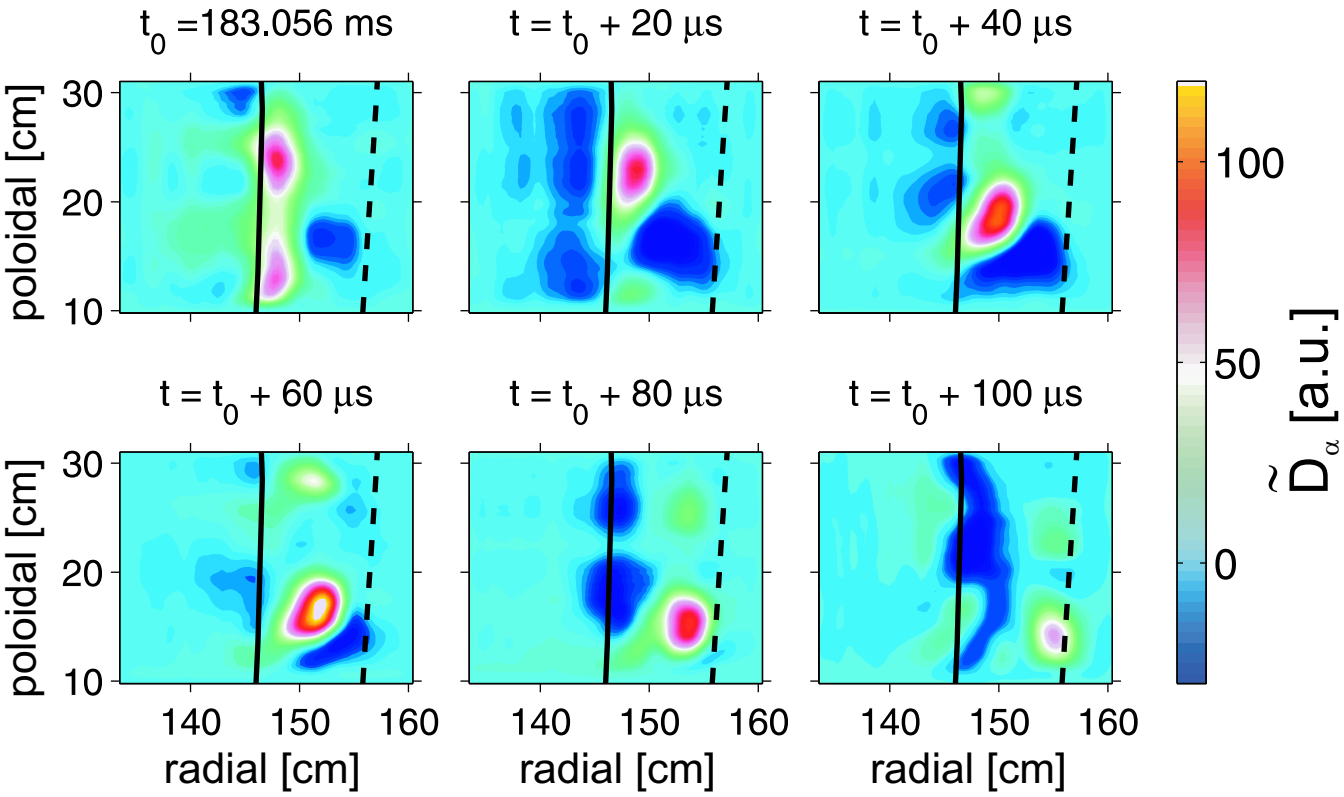

Figure 2. Pre-processed raw images of the PSI5 camera (shot 112724) where the dc-component $\bar{D}_\alpha$ is removed. A structure propagates from the separatrix (solid black line) across the SOL towards the limiter edge (dashed black line).

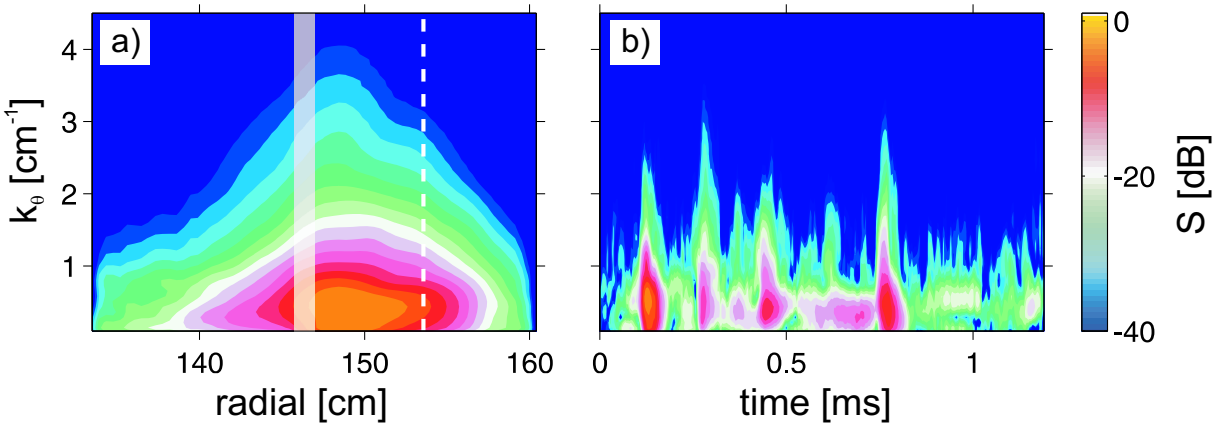

Figure 3. Time-averaged poloidal wavenumber spectra for the radial GPI field-of-view (a) and temporally resolved wavenumber spectrum for a discrete radial position in the SOL ($r = 153$ cm, b) for shot 113734. The shaded box in (a) indicates the separatrix position and the dashed line corresponds to the radial position of the spectrum shown in (b).

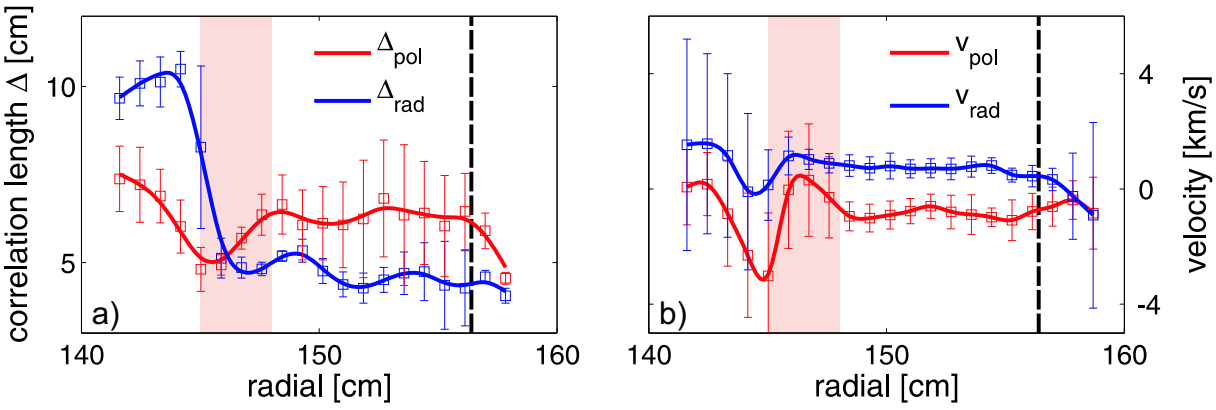

Figure 4. Radial evolution of the polodial (red) and radial (blue) correlation lengths (a) and fluctuation velocities (b) obtained from cross-correlation analysis of NSTX shot 113734. The error bars represent the standard deviation of the different poloidal reference probe positions (see text for details). The position of the separatrix is indicated by the red shaded box and the limiter edge is indicated by the dashed black line.

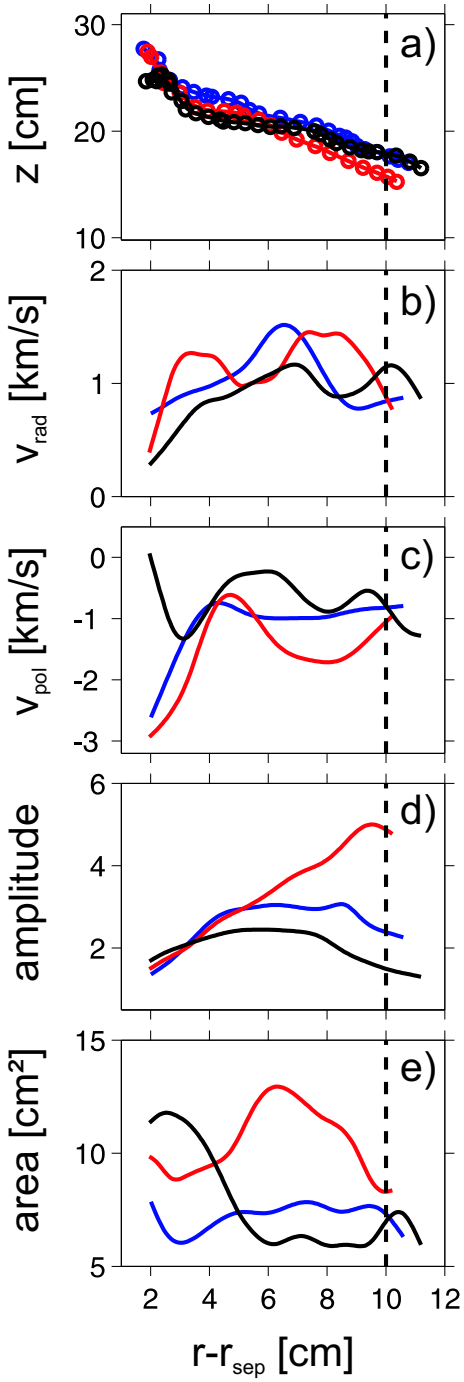

Figure 5. Specific properties for three long living individual structures propagating from the separatrix at $r - r_{sep} = 0$ to the limiter across the SOL. Shown are the structure trajectory (a), the radial (b) and poloidal (c) structure velocities, the evolution of the relative structure amplitude normalized to the time-averaged background $\bar{D}_\alpha$ emission (d) and the structure area (e). The dashed black line corresponds to the minimum radial position of the limiter edge.

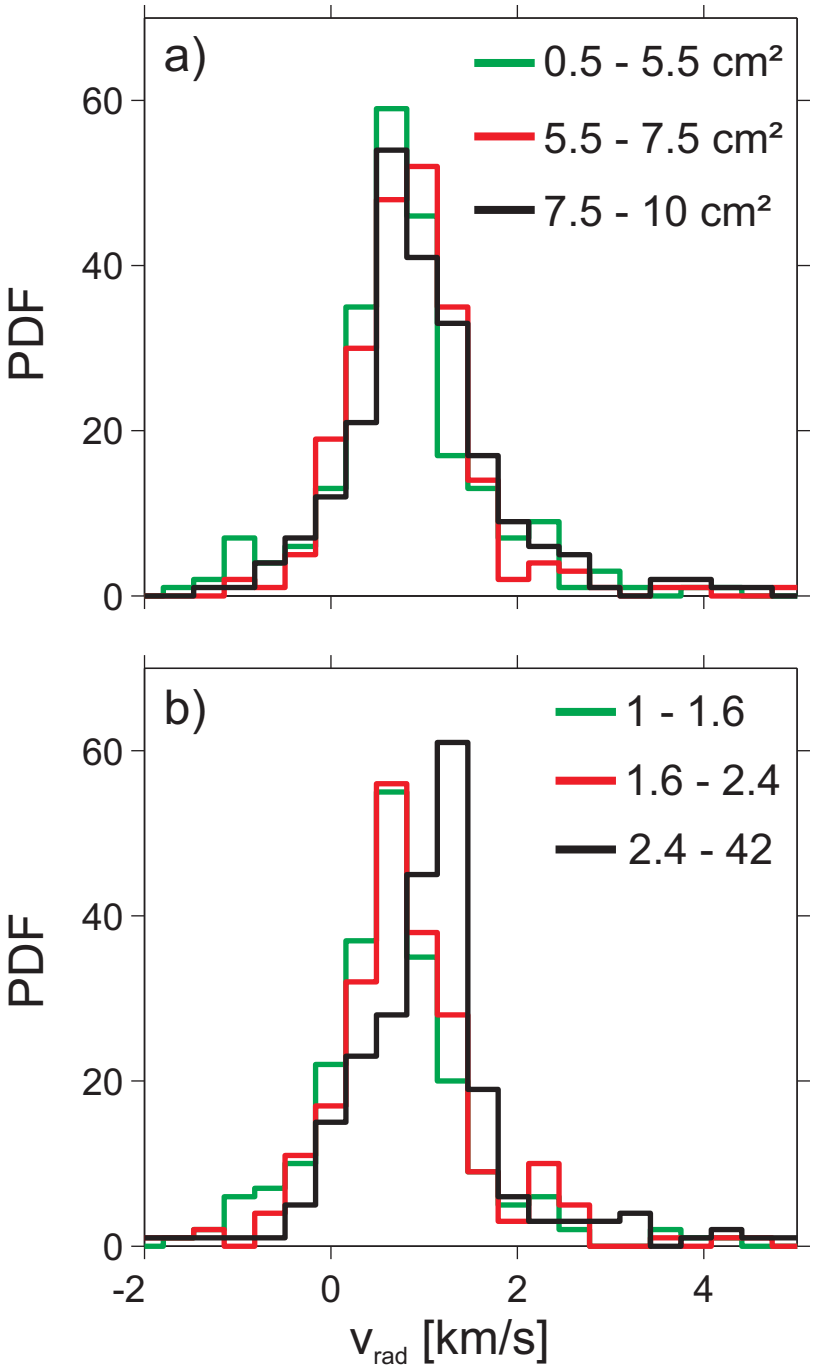

Figure 6. Probability distribution function (PDF) of the radial structure velocity in the plasma edge and SOL ($r - r_{sep} = 0 \ldots 10\,\mathrm{cm}$) for structures with different areas (a) and amplitudes normalized to $\bar{D}_\alpha$ (b). 230 structure ensembles contribute toe each PDF.

The Princeton Plasma Physics Laboratory is operated
by Princeton University under contract
with the U.S. Department of Energy.

Information Services
Princeton Plasma Physics Laboratory
P.O. Box 451
Princeton, NJ 08543

Phone: 609-243-2750
Fax: 609-243-2751
e-mail: pppl_info@pppl.gov
Internet Address: http://www.pppl.gov